



**HAL**  
open science

# Influence of the printing parameters on the stability of the deposited beads in fused filament fabrication of poly(lactic) acid

Shahriar Bakrani Balani, France Chabert, Valérie Nassiet, Arthur Cantarel

## ► To cite this version:

Shahriar Bakrani Balani, France Chabert, Valérie Nassiet, Arthur Cantarel. Influence of the printing parameters on the stability of the deposited beads in fused filament fabrication of poly(lactic) acid. Additive Manufacturing, 2019, 25, pp.112-121. 10.1016/j.addma.2018.10.012 . hal-03110529

**HAL Id: hal-03110529**

**<https://hal.science/hal-03110529>**

Submitted on 14 Jan 2021

**HAL** is a multi-disciplinary open access archive for the deposit and dissemination of scientific research documents, whether they are published or not. The documents may come from teaching and research institutions in France or abroad, or from public or private research centers.

L'archive ouverte pluridisciplinaire **HAL**, est destinée au dépôt et à la diffusion de documents scientifiques de niveau recherche, publiés ou non, émanant des établissements d'enseignement et de recherche français ou étrangers, des laboratoires publics ou privés.



## Open Archive Toulouse Archive Ouverte (OATAO)

OATAO is an open access repository that collects the work of some Toulouse researchers and makes it freely available over the web where possible.

This is an author's version published in: <http://oatao.univ-toulouse.fr/20922>

**Official URL:** <https://doi.org/10.1016/j.addma.2018.10.012>

### To cite this version:

Bakrani Balani, Shahriar and Chabert, France and Nassiet, Valérie and Cantarel, Arthur Influence of the printing parameters on the stability of the deposited beads in Fused Filament Fabrication of poly(lactic) acid. Vol. 25, pp. 112-121 (2019) Additive Manufacturing.

Any correspondence concerning this service should be sent to the repository administrator:

[tech-oatao@listes-diff.inp-toulouse.fr](mailto:tech-oatao@listes-diff.inp-toulouse.fr)

# Influence of printing parameters on the stability of deposited beads in fused filament fabrication of poly(lactic) acid

Shahriar Bakrani Balani <sup>1,2,a)</sup>, France Chabert <sup>1,b)</sup>, Valérie Nassiet <sup>1,c)</sup>, Arthur Cantarel <sup>2,d)</sup>,

<sup>1</sup> LGP-ENIT-INPT, University of Toulouse, 47 Avenue d'Azereix, BP1629-65016 Tarbes Cedex, France

Web Page: <http://www.enit.fr/>

<sup>2</sup> Institut Clément Ader (ICA), CNRS UMR 5312, University of Toulouse, IUT of Tarbes, UPS, France

Web Page: <http://www.institut-clement-ader.org/>

Corresponding author: <sup>b)</sup> [fchabert@enit.fr](mailto:fchabert@enit.fr)

<sup>a)</sup> [sbakrani@enit.fr](mailto:sbakrani@enit.fr)

<sup>c)</sup> [vnassiet@enit.fr](mailto:vnassiet@enit.fr)

<sup>d)</sup> [arthur.cantarel@iut-tarbes.fr](mailto:arthur.cantarel@iut-tarbes.fr)

## Abstract:

Fused filament fabrication (FFF) is one of the various types of additive manufacturing processes. Similar to other types, FFF enables free-form fabrication and optimised structures by using polymeric filaments as the raw material. This work aims to optimise the printing conditions of the FFF process based on reliable properties, such as printing parameters and physical properties of polymers. The selected polymer is poly(lactic) acid (PLA), which is a biodegradable thermoplastic polyester derived from corn starch and is one of the most common polymers in the FFF process. Firstly, the maximum inlet velocity of the filament in the liquefier was empirically determined according to process parameters, such as feed rate, nozzle diameter and dimensions of the deposited segment. Secondly, the rheological behaviour of the PLA, including the velocity field, shear rate and viscosity distribution in the nozzle, was determined via analytical study and numerical simulation. Our results indicated the variation in the shear rate according to the diameter of the nozzle and the inlet velocity. The shear rate attained its maximum value near the internal wall at high inlet velocities and smaller diameters. Finally, the distribution of the viscosity along the radius of the nozzle was obtained. At high inlet velocity, several defects appeared at the surface of the extrudates. At the highest shear rates, the extrudates underwent severe deformation. The defects predicted via numerical simulation were reasonably consistent with that observed from an optical microscope. Hence, these results are effective for selecting the printing parameters (i.e. nozzle diameter, feed rate and layer height) to improve the quality of the manufactured parts.

- Keywords

Additive manufacturing, fused filament fabrication, multiphysics numerical simulation, poly(lactic) acid, rheological behaviour.

## Introduction

Additive manufacturing refers to a wide variety of processes for manufacturing 3D complex shape parts. These emerging manufacturing technologies are sorted according to various criteria, such as

nature (powder or filament) of the raw material (metal, ceramic or polymer), deposition strategy and energy source. Among these processes, fused filament fabrication (FFF) is the most widely used process for thermoplastics. It has been brought to completion because of the contribution of numerous workers of FabLabs worldwide, as well as research studies by academics to obtain an in-depth understanding of the physical phenomenon.

In the FFF process, thermoplastic or metallic filaments (also called wires) are heated in a liquefier. The hot filaments are deposited layer by layer [1]. Among the machines available in the market, RepRap is an open-source project developed in 2007 to spread the use of the FFF process at a low cost for ‘home manufacturing’ and for FabLabs, as well to support education [2][3]. Furthermore, to ensure inexpensive and convenient manufacturing, these machines comprise a frame, a liquefier and open-source software. The liquefier is composed of several parts, such as a heating block, nozzle and cooling sink. Figure 1 shows a schematic of the liquefier assembly typically used for RepRap machines.

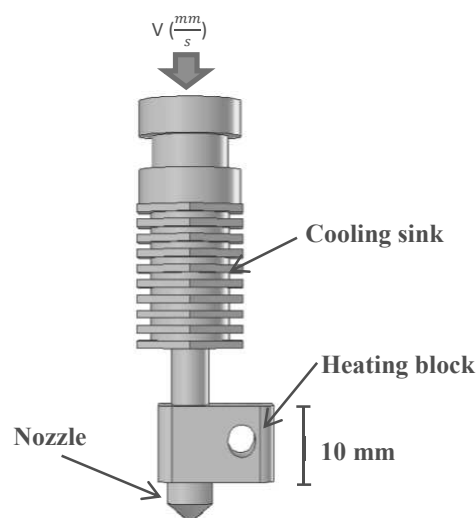


Figure 1: Extruder in RepRap FFF machines

Although these open-source printers provide robustness and low-cost manufacturing, the parts manufactured by using these printers still exhibit different flaws, such as low mechanical strength, high surface roughness and low dimensional accuracy. These drawbacks are the main results of the inadequate understanding of the material properties. A large number of users worldwide follow the ‘rule of thumb’ experimental practice to determine optimum printing parameters. The selection of an excessively high temperature and high printing speed through such means results in severe deformation and discontinuity of the printed layers, whereas an excessively low temperature results in incomplete melting of the filament and inadequate adhesion between the deposited filaments. Therefore, understanding the flow properties of the polymer during printing, as well as the influence of the printing parameters on the flow properties, is crucial for improving the quality of the manufactured parts.

In parallel to the experience gained by users, the first scientific studies aimed at improving the quality of the parts manufactured via the FFF process were conducted by Yardimici et al. in 1999 [4]. According to viscosity equations for non-Newtonian fluids, they proposed a relationship to determine the pressure drop in the liquefier [5]. The researchers have also proposed thermal equations to determine the temperature distribution in the liquefier and extruder [4] [5]. Most of the studies on FFF

focus on the deposition orientation and the influence of different filament deposition strategies and raster orientations on the mechanical properties of the parts printed via FFF, such as tensile strength [6] [7] [8] [9], compression [10] and flexural properties [6] [11] [12]. However, many numerous contradictions are apparent in these studies when researchers attempted to determine the optimum raster orientation of printed parts. A hypothesis to explain these contradictions can be the inadequate knowledge on the properties of polymers. Certain authors attributed this hypothesis to colour diversity [13] or supplier company variability.

Meanwhile, numerous studies have been conducted to measure and decrease the surface roughness of parts manufactured via the FFF process [14]. The influence of process variables, such as layer thickness, road width and deposition speed, on the surface quality of parts manufactured via FFF [15] [16] was observed. Hence, several post-processing treatments were proposed to decrease the surface roughness of these parts. Chemical post-processing treatment [17] [18] [19], modification of the generated code and slicing [19] [20] [21] and post-processing machining [22] are also effective to reduce the roughness. In a similar context, optical observations reveal that the quality of the curved geometry of parts fabricated via FFF is low, that is, the dimensions of the curved part do not accurately satisfy the specifications. Thus, an adequate slicing procedure is required to improve the quality of the curved regions [20] [21] [23].

Furthermore, the mechanical properties of the printed parts are established to directly link to the adhesion among the deposited filaments [24]. When the filaments are deposited one after the other, they bond together to form the layers. This physical phenomenon is called coalescence, which was extensively studied in other processes [25] and specifically applied to the FFF process by Bellehumeur et al. [26]. Coalescence is mainly governed by the viscosity and surface tension of polymers [27]. Understanding the temperature influence on the rheological properties of polymers is necessary to control and improve the coalescence of deposited beads.

For a number of decades, flow and heat transfer modelling has been a major concern in the study of polymer processing [28]. Through these works, the reliability and quality of industrial plastic products have been remarkably improved. During the FFF process, the filament passes through a liquefier before deposition, similar to the extrusion process. Notwithstanding numerous experimental works, only a few of them introduced the numerical simulation of polymer flow when it exits the liquefier. These approaches are generally based on the finite element method for the investigation of a single-phase flow, and they also are applied to extrusion and injection moulding [29].

With specific regard to our case, only a few works are worth to be cited. Lirvani [30] modelled the extrusion process of a fluid with the viscosity of approximately 20 Pa·s via numerical simulation and by using Navier–Stokes equation. Kopplmayr [31] used OpenFOAM software and volume of fluid (VOF) equations to model the extrusion of polyethylene, polypropylene and polyethylene terephthalate. The results of their numerical modelling are reasonably consistent with those of the experimental studies. Comminal [32] modelled the free-form extrusion of the polymer by using VOF equations and considering its viscoelastic behaviour. He observed the deformation of the extrudate. Bot [33] investigated the effect and solidification of a metal droplet on a substrate by using VOF and total variation diminishing. Nevertheless, his study involved a segregated droplet and the effect of this isolated droplet on the substrate, rather than a continuous deposition of a filament on a substrate. Amico et al. [34] determined the heat transfer in the FFF process via adaptable finite element analysis. However, the flow in their model was not directly simulated. The thermal behaviour of a liquefier in a RepRap 3D printer was investigated by Jerez-Mesa et al. [35]. They had stationary-modelled the fluid flow and temperature in the liquefier by using continuity equations. The work closest to ours was

conducted by Comminal [36]. The researcher modelled the behaviour of the extrudate for a viscoelastic material. He had also considered streamlines caused by the elastic instability in the die. A sharkskin phenomenon is known to be related to elastic instabilities in capillaries. Comminal [36] in the numerical approach considered the viscoelasticity to model the flow behaviour. To achieve this, he used VOF and log-conformation tensors. The same author [37] has modelled the material deposition on a substrate by modelling the fluid flow. This study highlighted the influence of geometry and inlet velocity on the cross-sectional form of the deposited bead via computational fluid dynamic simulation.

In our latest publication [38], the extrusion step in the FFF process was investigated via numerical simulation and by using two-phase flow (TPF) level set (LS) equations. The numerical simulation considered the rheological properties to track the front of the polymer extrudate during filament deposition. The fluid flow, temperature distribution and viscosity of the extrudate when it exits from the liquefier were calculated. Additionally, Peng et al. [39] experimentally studied the polymer flow in the FFF process. By using the pigments moving in the flowing fluid to trace the pathline, they determined the velocity distribution in the liquefier. Moreover, Osswald et al. [40] developed an analytical model for describing the melting of the filament in the FFF process. Their analytical model was based on the control of the polymer flow according to the force in the liquefier. They employed a thin polymer layer in the liquefier close to the nozzle and determined the pressure field in this thin layer when the diameter of the nozzle was changed. This model involves the initial temperature of the filament, heater temperature, applied force, nozzle tip angle, capillary diameter and length, as well as rheological and thermal properties.

Despite many attempts to understand the mechanical properties of parts manufactured via the FFF process, the absence of thorough studies is apparent. To our knowledge, the relationship between the printing parameters and the physical properties of polymers and the consequence on the viscosity and shape of the filament immediately before deposition are not yet clear. However, the rheological properties directly influence the mechanical properties of the printed parts by affecting the coalescence of the deposited beads [41] and the shape of the extrudate. As explained in the diagram of Figure 2, the printing parameters (i.e. nozzle diameter, feed rate and height of a layer) affect the inlet velocity in the liquefier and therefore the shear rate. On the basis of the shear rate in the liquefier and the physical properties of the polymer (thermal transitions and rheological behaviour), the viscosity field and the extrudate shape are predicted.

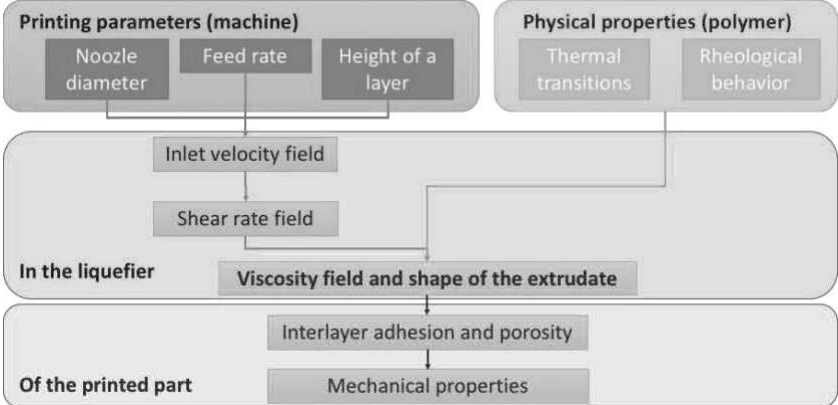


Figure 2: Diagram of the printing parameter effects and physical properties of the polymer on the mechanical properties of printed parts. The temperature of the heater is also used as one of the printing parameters, but it is not mentioned in the diagram because it does not directly affect on the inlet velocity field.

The present study aims to link the printing parameters and the physical properties of the polymer to the viscosity and the shape of the filament immediately before deposition in the FFF process. The study's originality is that it proposes a time-dependent numerical approach that also addresses the changes in the rheological properties with respect to the changes in the shear rate and temperature. In this work, the poly(lactic) acid (PLA) was selected. In the first part, the physical properties (thermal transitions and rheological properties) of the PLA were determined. In the second part, a relation was proposed to determine the inlet velocity of the polymeric filament in the liquefier according to the printing parameters (i.e. nozzle diameter, feed rate and height of a layer). Then, the inlet velocity field, shear rate field and viscosity of the PLA for the printing parameters were determined via numerical simulation and analytical study. Finally, the influence of the shear rate on the extrudate shape was investigated via experiment and numerical simulation.

## Materials and methods

The measurement of pressure and shear rate are not feasible in commercial 3D and RepRap printers. Therefore, a laboratory extruder was used to represent the fluid flow in a printer as close as feasible. The experimental study was conducted using an extruder system from Thermo Fisher Company. As shown in Figure 3(a), the extruder has three units. The driver unit is HAAKE PolyLab OS, and the extruder unit is HAAKE Rheomex OS equipped with a single screw with a maximum rotating speed of 150 rpm. Meanwhile, the third part is a gear pump, that is, HAAKE Melt pump OS with a maximum speed of 75 rpm. At the outlet of the extruder, a 0.5-mm diameter die is used to represent the nozzle; its geometry is shown in Figure 3(b).

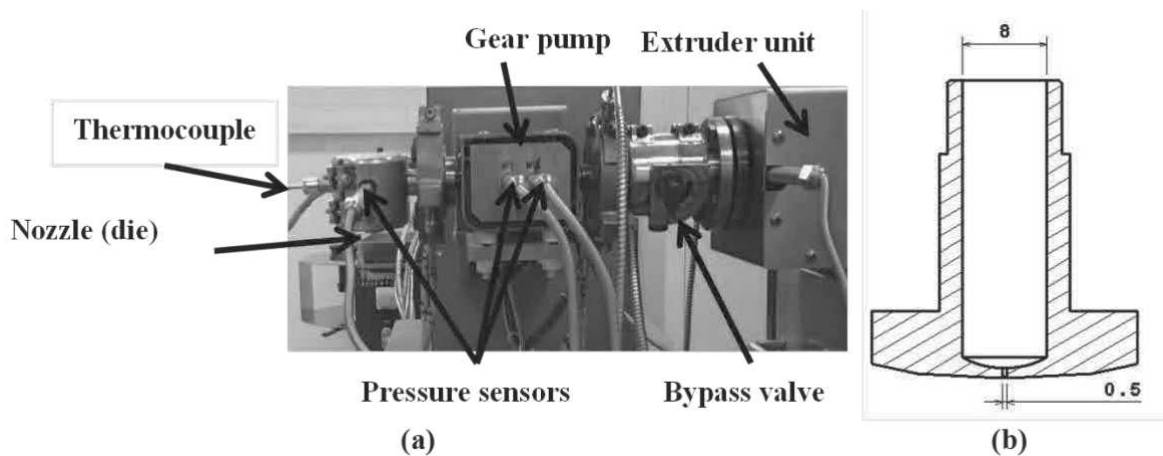


Figure 3: (a) Extruder system used for the experimental study. (b) Scheme of the 0.5-mm diameter nozzle

The PLA (NaturePlast PLI 005) in pellets was for the experimental study. The PLA filaments for 3D printers were formulated with additives to tune their properties. Nevertheless, we opted to work with a PLA of the highest feasible purity for a better understanding of the phenomena. The density of the PLA in its melted state is  $1250 \text{ kg}\cdot\text{m}^{-3}$  according to the technical datasheet provided by the manufacturer [42] [43]. The polymer was dried for 3 h in an oven at  $T = 60 \text{ }^\circ\text{C}$  to remove its moisture before processing.

The glass transition ( $T_g$ ) and melting temperature ( $T_m$ ), as well as the kinetics of crystallisation of the PLA, were determined using differential scanning calorimeter (DSC) Q200 from TA Instrument. All the DSC experiments were performed at  $10 \text{ }^\circ\text{C}\cdot\text{min}^{-1}$  under nitrogen flow with an approximate sample weight of 10 mg.

The rheological properties of the PLA were determined using the ARES-LN2 rheometer from Rheometrics. The experiments were performed under an air flow using a 25-mm diameter parallel-plate configuration. All the tests were conducted in an oscillatory mode in the viscoelastic linear domain, determined previously from strain sweep tests. The storage ( $G'$ ) and loss moduli ( $G''$ ), as well as the alpha transition temperature ( $T\alpha$ ), which is the rheological effect of  $T_g$ , were measured. The dynamic complex viscosity  $\eta^*$  was calculated from the storage and loss moduli by using equation (1) with the angular frequency  $\omega$ :

$$\eta^* = \frac{\sqrt{G'^2 + G''^2}}{\omega} \quad (1)$$

## Theoretical basis

### Rheological investigation of the polymer flow in the liquefier via analytical study

When the printing conditions, such as nozzle diameter and feed rate, vary, the inlet velocity and hence the shear rate change. Consequently, the viscosity of the fluid was also changed. Therefore, determining these properties and the influence of their variations on the quality of the manufactured part are important. Experimental observations revealed that a higher viscosity results in liquefier clogging and a low viscosity causes inaccurate dimensions, low quality of the deposited filament and liquefier leakage. The filament undergoes temperature variations during the process. Hence, the temperature distribution directly influences the viscosity of the polymer in the liquefier.

All melted thermoplastic polymers demonstrate a shear-thinning behaviour. The viscosity of shear-thinning fluids changes with temperature and shear rate, and the latter is related to the inlet velocity of the fluid in the liquefier. In the present section, the analytical equations for determining the variation of the viscosity in the liquefier for non-Newtonian fluids are explained.

For non-Newtonian fluids, the viscosity can be expressed in the most convenient form of a power law or by using the Carreau–Yasuda model which considers the Newtonian plateau at low shear rates. The viscosity according to the shear rate is expressed by equation (2), following the power law equation [44][45].

$$\eta = K|\dot{\gamma}|^{n-1} \text{ for shear – thinning fluids } (n < 1), \quad (2)$$

where  $n$  is the pseudoplasticity index,  $K$  is the consistency coefficient and  $\dot{\gamma}$  is the shear rate. By reversing the pseudoplasticity index, the fluidity constant  $\varphi$  is determined using equations (3) and (4). The parameter  $n$ , called ‘the pseudoplasticity index’, is the slope of the viscosity versus the shear rate curve. When the pseudoplasticity is above one, the fluid exhibits a shear-thickening behaviour. When the pseudoplasticity index is below one, the fluid exhibits a shear-thinning behaviour, where  $K$  is the viscosity at the shear rate of  $1 \text{ s}^{-1}$ . The reciprocal of viscosity is generally called ‘fluidity’.

$$n = \frac{1}{m} \quad (3)$$



$$K = \varphi^{-\frac{1}{m}} \quad (4)$$

The fluidity constant  $\varphi$  represents the capability of the fluid to flow. Meanwhile, the viscosity of non-Newtonian fluid can be expressed as the Carreau–Yasuda model, which is represented in equation (5).

$$\eta = \eta_{inf} + (\eta_0 - \eta_{inf})[1 + (\lambda\dot{\gamma})^a]^{\frac{n-1}{a}}, \quad (5)$$

where  $\eta_0$  is the viscosity of the fluid at zero shear rate,  $\eta_{inf}$  is the viscosity of the fluid at infinite shear rate,  $\lambda$  is the relaxation time index,  $n$  is the power index,  $a$  is a dimensionless parameter describing the transition between the first Newtonian plateau and the power law zone and  $\dot{\gamma}$  the shear rate. Irrespective of whether the equation is based on the power law or Carreau–Yasuda model, the viscosity was revealed to decrease when the shear rate increases. The shear rate dependency varies with the nature of the polymer, the temperature and the velocity field in the geometry. Furthermore, the temperature is regarded as constant with time at a fixed point in the FFF system.

For a shear-thinning fluid, the flow in the extruder is a Hagen–Poiseuille flow. Thus, the flow has a parabolic shape, implying that the velocity attains its maximum value at the centre of the nozzle. Meanwhile, the value of the velocity field near the internal wall is zero. For non-Newtonian fluid, the fluid velocity can be determined using equation (6) [46].

$$u(r) = \frac{3n+1}{n+1} \bar{V} \left[ 1 - \left( \frac{r}{R} \right)^{\frac{(1+n)}{n}} \right], \quad (6)$$

where  $\bar{V}$  is the average inlet velocity of the fluid in the liquefier,  $r$  is the distance from the centre of the nozzle,  $R$  is the nozzle radius and  $n$  is the power index in the Carreau–Yasuda model. The shear rate is determined by determining the velocity based on the radius of the internal nozzle diameter, which can be expressed in equation (7).

$$\dot{\gamma} = \frac{du}{dr} = \frac{3n+1}{nR} * \bar{V} * \left[ \left( \frac{r}{R} \right)^{\frac{1+n}{n}-1} \right] \quad (7)$$

Finally, the maximum shear rate, located at the internal wall of the nozzle, is obtained using equation (8).

$$\dot{\gamma}_w = \frac{8(3n+1)Q}{n*\pi D^3} = \frac{(3n+1)\bar{V}}{nR}, \quad (8)$$

where  $Q$  is the volumetric flow rate and  $D$  is the diameter of the nozzle.

### Numerical simulation by COMSOL Multiphysics

In the present study, the numerical simulation of the extrusion process was performed using the TPF simulation of the COMSOL Multiphysics software. The LS and Navier–Stokes equations were used to determine the rheological properties of the flow with a focus on the time when the extrudate exits from the extruder nozzle.

For each phase in the LS method, the Navier–Stokes and continuity equations were solved for the conservation of momentum and mass [33]. Equation (9) expresses the general form of the Navier–Stokes equation.

$$\overbrace{\rho \frac{\partial u}{\partial t} + \rho(u \cdot \nabla u)}^1 = \nabla \cdot \left[ \overbrace{-pI}^2 + \overbrace{\mu(\nabla u + (\nabla u)^T - \frac{2}{3}\mu(\nabla \cdot u)I)}^3 \right] + \overbrace{\rho g + F_{st} + F}^4 \quad (9)$$

where  $\rho$  is the density,  $u$  is the flow velocity,  $P$  is the pressure applied to the fluid,  $\mu$  is the dynamic viscosity of the fluid,  $g$  is the gravity field,  $F_{st}$  represents the force resulting from the surface tension and  $F$  represents all other external forces. The Navier–Stokes equations correspond to the contribution of different forces applied to the fluid. Term 1 of equation (9) refers to the inertial forces of the fluid. The influence of the pressure and viscous forces were integrated into the equation by terms 2 and 3, respectively. Term 4 is the sum of other external forces applied to the fluid. The mass conservation in the study is solved using the continuity equation.

$$\rho(u \cdot \nabla u) = 0 \quad (10)$$

For the flows in very low Reynolds number, the inertial term in the Navier–Stokes equation can be omitted. Finally, the Navier–Stokes equation used in the study is simplified and transformed as equation (11).

$$\rho \frac{\partial u}{\partial t} = \nabla \cdot [-pI + \mu(\nabla u + (\nabla u)^T)] + \rho g + F_{st} + F \quad (11)$$

The Navier–Stokes and continuity equations were solved for the conservation of momentum and mass, respectively. The density  $\rho$  and viscosity  $\mu$  of the fluids in the system were determined using equation (13). In the TPF simulation, the interface of the two fluids was tracked by solving an additional transport equation. This transport equation for the LS method used in the COMSOL Multiphysics for tracking the interface of two phases is represented by equation (12).

$$\frac{\partial \varphi}{\partial t} + \nabla \cdot (u\varphi) = \gamma \nabla \cdot \left( \varepsilon_{ls} \nabla \varphi - \varphi(1 - \varphi) \frac{\nabla \varphi}{|\nabla \varphi|} \right) \quad (12)$$

where  $t$  is the time,  $u$  is the flow velocity,  $\varphi$  is the volume fraction,  $\gamma$  is the re-initialisation parameter and  $\varepsilon_{ls}$  is the parameter regulating the interfacial thickness. The re-initialisation parameter ( $\gamma$ ) is considered to be the maximum or close to the maximum velocity of the fluid in the TPF system to ensure the consistency of the results with the entire set of simulations. The thickness of the interface between two phases was minimized by reducing  $\varepsilon_{ls}$  for the clarity between the phases.

We present here a system of three equations, that is, equations (10), (11) and (12), and three unknowns. The unknowns are the velocity in the x and y directions and the volume fraction ( $\varphi$ ). Meanwhile, the known parameters are density, viscosity and inlet velocity (or pressure). By using the Navier–Stokes and LS equations, the unknowns were determined in each time. At  $t = 0$ , the initial value of  $\varphi$  in the system is zero for the air and one for the polymer, and the parameters are the viscosity and density of the polymer in the system.

The volume fraction is the parameter which regulates the interface. In the TPF simulation, the density and viscosity of each mesh of the system were determined using equation (13), according to the volume fraction  $\varphi$ .

$$\begin{aligned} \rho &= \varphi \rho_2 + (1 - \varphi) \rho_1 \\ \mu &= \varphi \mu_2 + (1 - \varphi) \mu_1 \end{aligned} \quad (13)$$

where  $\rho_1$  and  $\rho_2$  are the densities of phases 1 and 2, respectively, and  $\mu_1$  and  $\mu_2$  are the viscosities of phases 1 and 2, respectively. The volume fraction is one of the outputs of TPF simulation that is used for clearing the interface of the two phases. The colour legend of the volume fraction in TPF is blue for  $\varphi = 0$  and red for  $\varphi = 1$ . Hence, when the value of the colour function is 1 (or it is red), a polymer is present in the system or that this mesh is filled by polymer. Meanwhile, when the value of the volume fraction is 0 (or it is blue), air is present in the system or the mesh is filled by air.

When the extrudate exits from the nozzle, the density and viscosity of the system change according to the boundary conditions. The new viscosity and density of the system were calculated using equation (13). The results of the calculation of viscosity and density were re-inserted in equations (10), (11) and (12) to determine the new values of the unknowns. This iteration was applied until the completion of the simulation.

For the numerical simulation in the COMSOL Multiphysics default, physics-controlled meshes with predefined finer size and free triangular were selected. Figure 4 shows the boundary conditions used for the numerical simulation. For the subsequent numerical simulations, the density and viscosity of the air were set to  $1.225 \text{ kg}\cdot\text{m}^{-3}$  and  $1.8 \text{ }\mu\text{Pa}\cdot\text{s}$ , respectively.

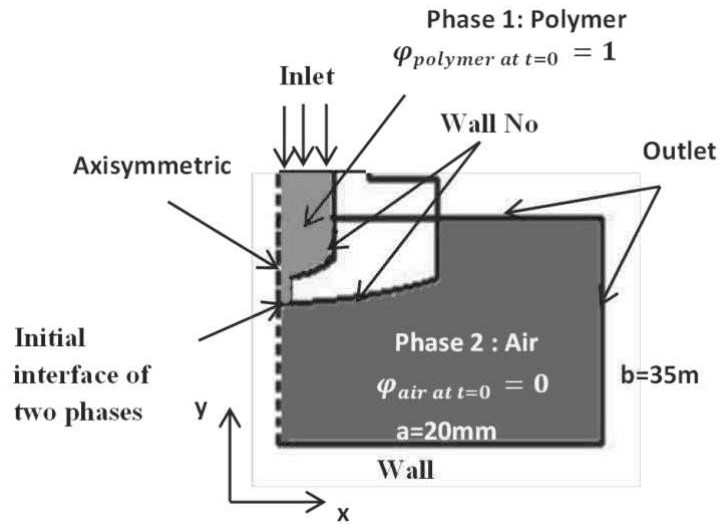


Figure 4: Geometry and boundary conditions used for the TPF numerical simulation

## Results and discussion

### Physical properties of the PLA

The glass transition, melting and crystallisation temperatures of the PLA were determined from the DSC curve shown in Figure 5. The results are compiled in Table 1. The measured glass transition temperature of the polymer was  $60 \pm 5$  °C. During the first heating of the raw PLA, no exothermic peak was observed. The complete melting of the polymer occurred between 160 °C and 170 °C, with an endothermic peak of  $57 \pm 3$  J·g<sup>-1</sup> representing the melting enthalpy. Given that the melting enthalpy of the 100% crystallised PLA was 93 J·g<sup>-1</sup> [47][48][49], the total crystalline rate was 61%.

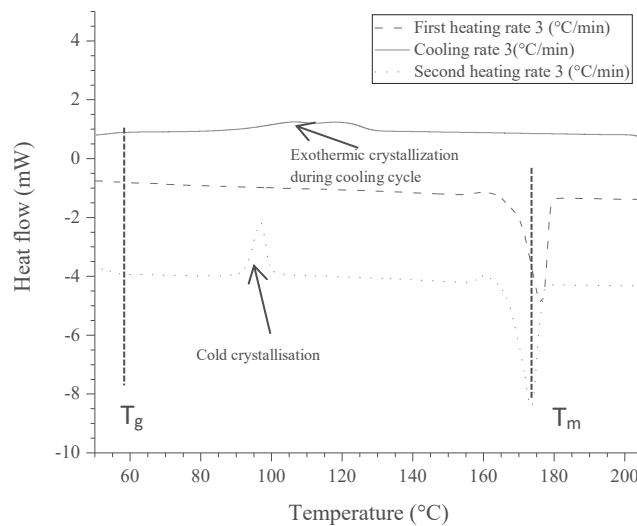


Figure 5: DSC curve of the PLA

For a semi-crystalline polymer, the crystallisation rate directly influences the mechanical properties. Owing to the organisation level, a higher crystalline rate results in higher Young's modulus [50]. As an evidence, to improve the strength of printed parts, the crystalline rate must achieve its maximum

value, determined previously as 61%. Furthermore, during the cooling cycle of  $3\text{ }^{\circ}\text{C}\cdot\text{min}^{-1}$ , an exothermic peak of approximately  $22 \pm 4\text{ J}\cdot\text{g}^{-1}$  was observed, indicating the kinetics in the PLA crystallisation. When the filament is deposited, the cooling rate below  $3\text{ }^{\circ}\text{C}\cdot\text{min}^{-1}$  must be applied to ensure a completely crystallised PLA, resulting in enhanced rigidity of the printed parts.

Figure 6(a) shows the curves of the dynamic complex viscosity of the PLA versus the angular frequency at different temperatures. The temperatures were selected according to the DSC results in Figure 5 to ensure that the polymer melted completely. Because of the rapid degradation of the PLA at low frequency, determining the complex viscosity at low frequencies where the measurement lasts for more than 10 min is infeasible. The viscosity of the PLA decreased dramatically for the frequencies below  $0.1\text{ rad}\cdot\text{s}^{-1}$  because the PLA degraded owing to macromolecular chain breakage during the measurements. To address this issue, the frequency range was extended to lower frequencies by applying the time–temperature equivalence to the storage and loss moduli. It involves shifting of the  $G'$  and  $G''$  curves obtained at the higher temperatures to the lower frequencies according to the reference temperature selected hereby as  $175\text{ }^{\circ}\text{C}$ . The master curve obtained for  $175\text{ }^{\circ}\text{C}$  is represented in Figure 6(b).

Table 1: Summary of DSC results of the PLA

Signs	Description	Value at the first heating ramp	Value at the cooling ramp	Value at the second heating ramp
$\Delta H_m$	Melting enthalpy	$57 \pm 3\text{ J}\cdot\text{g}^{-1}$	/	$51 \pm 2\text{ J}\cdot\text{g}^{-1}$
$\Delta H_c$	Crystallisation enthalpy	/	$22 \pm 4\text{ J}\cdot\text{g}^{-1}$	$20 \pm 3\text{ J}\cdot\text{g}^{-1}$
$T_m$	Melting temperature	$160\text{--}170\text{ }^{\circ}\text{C}$	/	$160\text{--}170\text{ }^{\circ}\text{C}$
$T_g$	Glass temperature	$60 \pm 5\text{ }^{\circ}\text{C}$	$60 \pm 5\text{ }^{\circ}\text{C}$	$60 \pm 5\text{ }^{\circ}\text{C}$

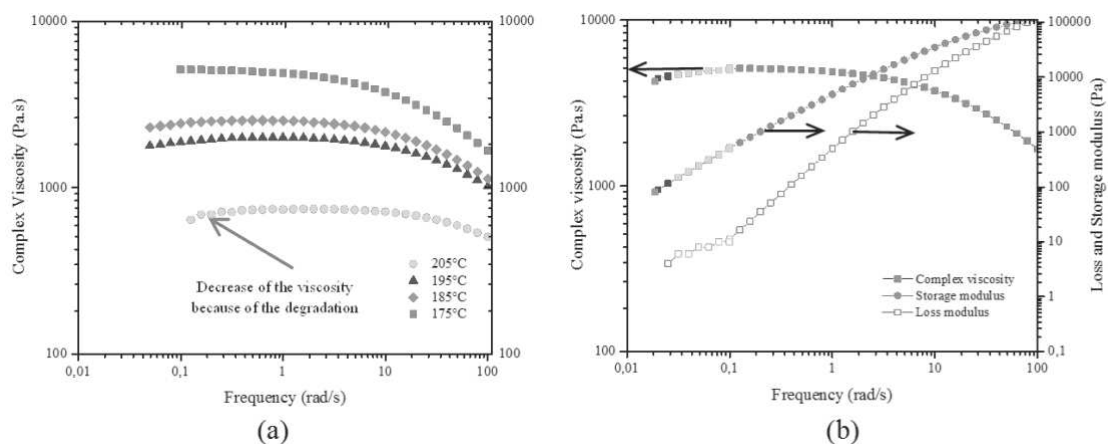


Figure 6: (a) Complex viscosity curves of the PLA. (b) Master curve for time–temperature equivalence for  $T = 175\text{ }^{\circ}\text{C}$

The slopes of  $G'$  and  $G''$  are 1.43 and 0.88, respectively (determined using a linear fitting), indicating that the terminal regime, where the slopes are typically two for  $G'$  and one for  $G''$ , has not been attained in our experimental range.

The viscosity curves were fitted with the Carreau–Yasuda equation by using the Origin software. The terms of the Carreau–Yasuda equation for the investigated temperatures are presented in Table 2. The Carreau–Yasuda model with these terms was implemented in the software to determine the flow properties in the liquefier.

Table 2: Values of terms of Carreau–Yasuda model for the viscosity curve fitting

	175 °C	185 °C	195 °C	205 °C
$\eta_0$	5169 ± 5	2480 ± 14	1945 ± 16	726 ± 6
$\eta_{inf}$	0	0	0	0
$\lambda$	0.048 ± 0.02	0.09 ± 0.5	0.08 ± 0.02	0.05 ± 0.01
<b>a</b>	0.82 ± 0.3	1.6 ± 0.8	1.931 ± 0.5	2.60 ± 0.01
<b>n</b>	0.52 ± 0.3	0.7 ± 0.3	0.693 ± 0.2	0.79 ± 0.11

### Inlet velocity in the liquefier

Our optical observations and empirical investigations of the shape of the deposited beads revealed that the shape of the section of the filament was changed from the initial circular to an elongated oval shape during printing. Figure 7 shows the final cross section of a deposited bead. The height of a layer,  $h$ , is one of the printing parameters.

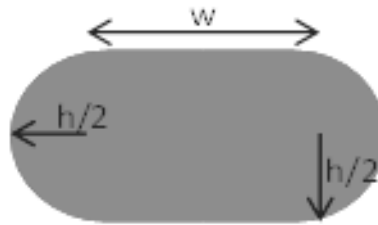


Figure 7: Cross section of a deposited bead

Considering the volume conservative law, the volume of the deposited bead was identical to that of the material exiting from the nozzle. Consequently, the inlet velocity of the polymer in the liquefier can be obtained as a function of the printing parameters, as expressed by equation (14).

$$v = \frac{4f}{\pi D^2} \left( wh + \frac{\pi h^2}{4} \right) \quad (14)$$

where  $v$  is the inlet velocity of the polymer in the liquefier,  $h$  is the height of the deposited segment,  $f$  is the feed rate,  $D$  is the nozzle diameter and  $w$  is the width of the deposited segment. A nozzle of 0.5-mm diameter was selected for our experimental study. The printing parameters selected for this study are presented in Table 3.

**Table 3: Values of the printing parameters**

Notations	Printing parameters	Values and units
<b>D</b>	Diameter of the nozzle	0.5 mm
<b>H</b>	Height of the layer	0.7 mm
<b>F</b>	Feed rate	30 mm·s <sup>-1</sup>
<b>w</b>	Width of the bead	0.5 mm

### Shear rate and viscosity of the polymer in the liquefier:

The average inlet velocity ( $v$ ) was determined using equation (14) according to the printing parameters presented in Table 3. The inlet velocity field, shear rate field and viscosity of the polymer in the liquefier were determined via numerical simulation and analytical study for  $T = 195$  °C and a flow rate of  $18.5 \text{ cm}^3 \cdot \text{s}^{-1}$  according to the average inlet velocity.

The experimental study revealed that the PLA flowed easily at temperatures higher than 200 °C. At lower temperatures (i.e. 175 °C), the PLA underwent partial melting of the polymer pellets in the extruder screw, resulting in the blending of fluid and solid polymers. The DSC curve in Figure 5 shows that the PLA was completely melted at 180 °C. At 185 °C, the polymer was melted but the viscosity remained very high. Consequently, a high torque was applied to induce the PLA flow, which exceeded the limit of the apparatus. Moreover, in the RepRap open-source printers, the printing temperature was generally 195 °C. Hence, the printing temperature of 195 °C was selected for the experiment, as described in the present section.

Figure 8 highlights the influence of the nozzle diameter (one of the printing parameters) on the inlet velocity, shear rate and viscosity in the liquefier at  $T = 195$  °C. The results obtained via numerical simulation and analytical studies were consistent. For example, at a fixed flow rate and temperature, the inlet velocity and shear rate varied from 4 to 484  $\text{mm} \cdot \text{s}^{-1}$  and from 27 to 7800  $\text{s}^{-1}$ , respectively, when the nozzle diameter was changed from 2 mm to 0.3 mm. Similarly, the nozzle diameter highly influenced the viscosity. The maximum value of the viscosity was determined to be 1850 Pa·s (nozzle diameter of 2 mm), whereas the minimum value of the viscosity was 295 Pa·s (nozzle diameter of 0.3 mm).

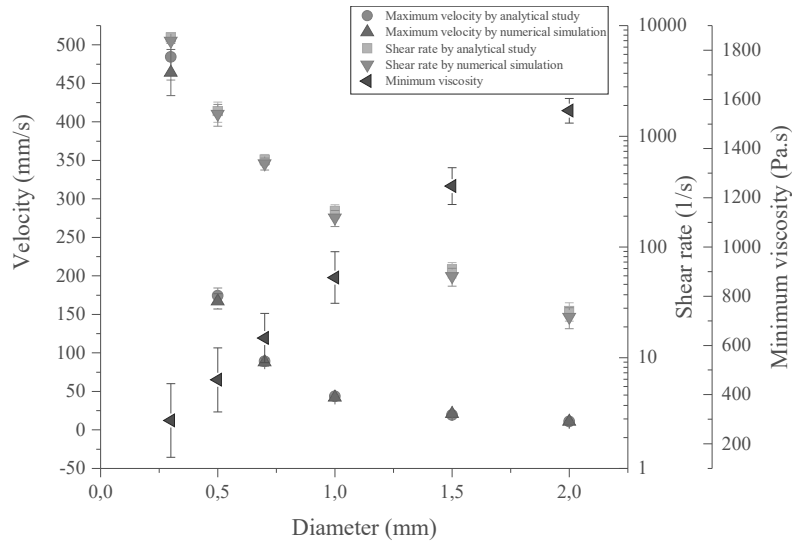


Figure 8: Influence of nozzle diameter on inlet velocity, shear rate and viscosity of the PLA at T = 195 °C

In most printers, the nozzle diameter is 0.3 mm or 0.5 mm. A nozzle of diameter 0.5 mm was selected for our experimental study. Figure 9 shows the distribution of the inlet velocity, shear rate and viscosity fields for the nozzle diameter of 0.5 mm.

The distribution of the inlet velocity in the liquefier (assimilated to a tube) exhibited a large difference between the maximum and minimum values. The maximum value of the velocity in the liquefier was  $160 \text{ mm}\cdot\text{s}^{-1}$  (at the centre), whereas its minimum value was zero (near the internal wall of the liquefier). The value zero was expected as it corresponded to the imposed condition of adhesion at the wall of the tube (not slippery). The shear rate changed from zero at the centre of the liquefier to  $1600 \text{ s}^{-1}$  near the internal surface of the liquefier. Consequently, near the internal wall, the viscosity attained its minimum value of approximately  $400 \text{ Pa}\cdot\text{s}$ , whereas at the centre of the tube, the viscosity was at its maximum value, that is, approximately  $1900 \text{ Pa}\cdot\text{s}$ . Hence, the results obtained via numerical simulation are in good agreement with that obtained via analytical studies.

The viscosity variation from the internal wall up to the centre of the liquefier was rapid because the viscosity at the centre of the liquefier was at its Newtonian plateau. Moreover, the profile of the shear rate of the material in the liquefier has a parabolic shape. The viscosity near the internal wall of the nozzle is at its minimum value, whereas at the centre of the nozzle, the viscosity reaches its maximum value. The parabolic shape of the shear rate profile illustrates the shear-thinning behaviour of the PLA according to equation (8).



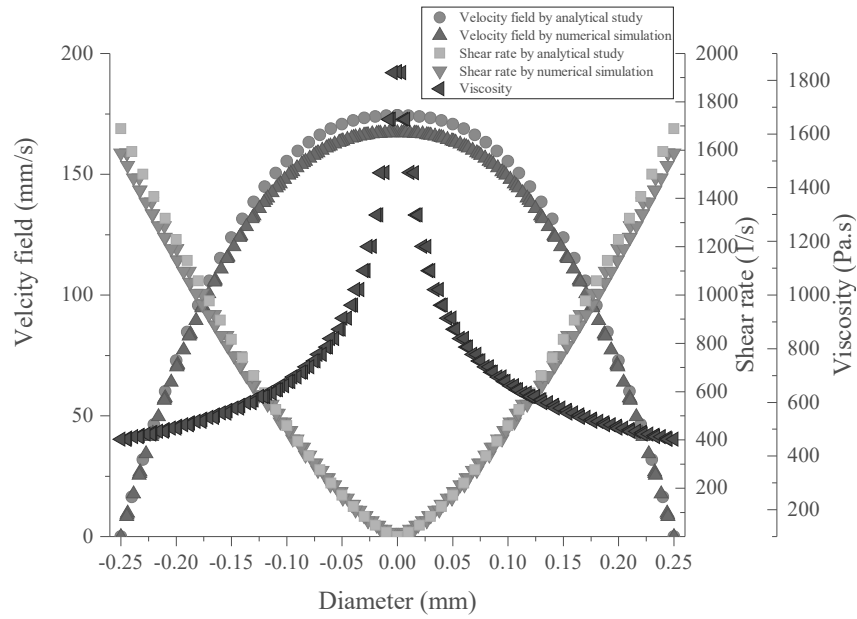


Figure 9: Distribution of velocity field, shear rate and viscosity in the liquefier determined via numerical simulation and analytical study

We now focus on the variation in the viscosity in the liquefier with respect to the distance from the centre of the nozzle. The numerical simulation revealed that when the temperature increases, the difference between the maximum value of the shear rate and its minimum value decreases.

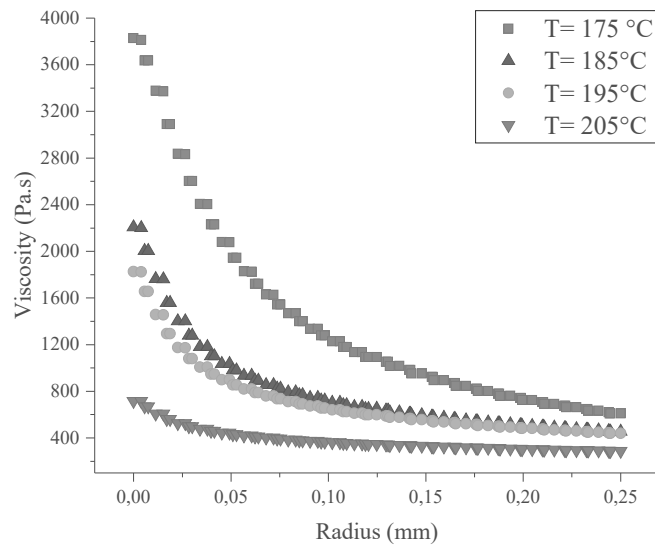


Figure 10: Distribution of the viscosity along the radius in the liquefier at various temperatures

Figure 10 shows the variation in the viscosity in the liquefier according to the distance from the centre of the nozzle at various temperatures for an inlet velocity of  $95 \text{ mm}\cdot\text{s}^{-1}$ . Irrespective of the temperature, the fluid demonstrates a shear-thinning behaviour. A comparison of the viscosity of the polymer at a high temperature (i.e.  $205 \text{ }^\circ\text{C}$ ) and at low temperature (i.e.  $175 \text{ }^\circ\text{C}$ ) for the same inlet velocity and nozzle diameter revealed that when the temperature increases, the difference between the maximum and minimum values of the viscosity decreases. Hence, for  $T = 175 \text{ }^\circ\text{C}$ , the difference between the maximum and minimum viscosity was approximately  $2800 \text{ Pa}\cdot\text{s}$ , whereas for  $T = 205 \text{ }^\circ\text{C}$ ,

this difference was approximately 400 Pa·s. Interestingly, for temperatures higher than 200 °C, the variation in the viscosity according to the shear rate was weak, as shown in Figure 9. For example, at 205 °C, when the polymer flows easily, the maximum viscosity at its Newtonian plateau was approximately 700 Pa·s, whereas at very high shear rates (more than 1000 s<sup>-1</sup>), it was approximately 400 Pa·s.

High fluidity of the polymer at high temperatures (> 205 °C) directly influences the quality of the printed parts. When the viscosity is low, the coalescence of the beads would be better because the macromolecules exhibit higher mobility required to diffuse and to create entanglements. However, high fluidity results in low accuracy during the deposition of the beads. A deposited bead undergoes creep phenomena with its weight, thereby causing low dimensional accuracy of printed parts, such as holes and extreme roughness. At high temperature, when the viscosity is excessively low, extra-supports of the parts are necessary to print complex shapes.

### **Influence of shear rate on extrudate shapes**

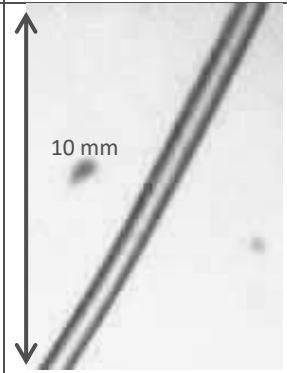
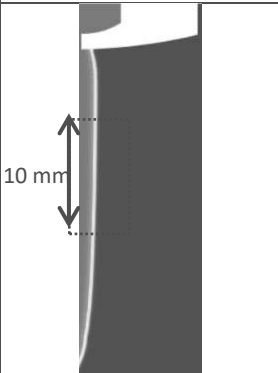
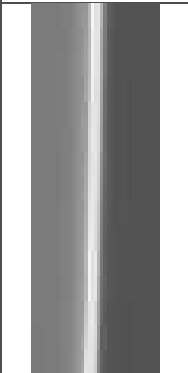
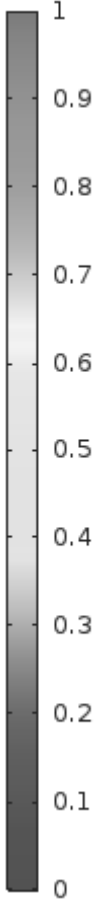
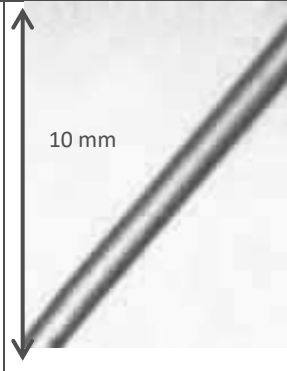
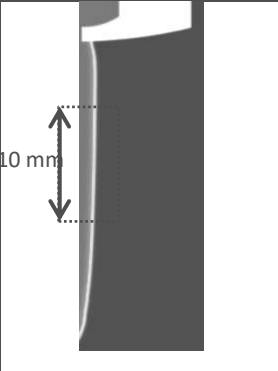
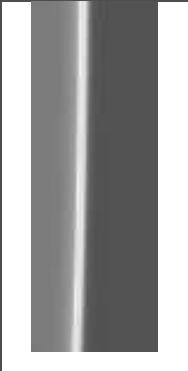
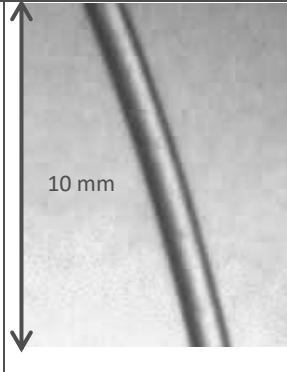
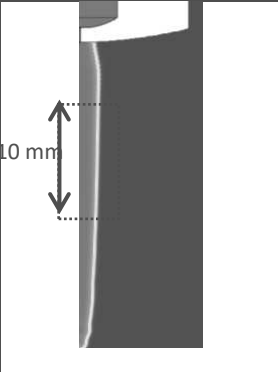
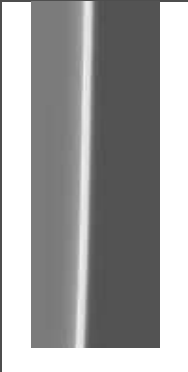
The polymer flow from the nozzle was regulated by controlling the speed of the pump during the experimental tests. Consequently, to precisely determine the shear rate, the weight flow rate was measured by cutting the extrudates at a constant time lapse. Then, the extrudates were weighted. By using the density of the PLA (1.25 g·mm<sup>-3</sup>), the weight flow rate was converted to volumetric flow rate. Finally, the volumetric flow rate was converted to the shear rate and inlet velocity by using equations (6)–(8).

An identical procedure was applied for various pump speeds. Thereafter, the extrudates were observed under an optical microscope. The images of the extrudates obtained at the different inlet velocities and shear rates at an isothermal of 195 °C are presented in Figure 11. The shape of the extrudates obtained via experimental study and numerical simulation were compared.

The influence of the shear rate on the shape of the extrudates was determined to be from 1200 s<sup>-1</sup> to more than 5000 s<sup>-1</sup>. The optical observations revealed that for the lowest shear rates, the shape of the extrudate was cylindrical with a smooth surface, whereas at higher shear rates and inlet velocities, deformations were observed on the surface. The limit appeared to be approximately 4000 s<sup>-1</sup>. Below this value, the shape of the extrudate became regular, whereas when the shear exceeded 4000 s<sup>-1</sup>, the flow was unstable, and the extrudate displayed defects. At 4100 s<sup>-1</sup>, some macroscopic instability was observed on the extrudate. At high shear stresses, the contour of the stream changed abruptly from that of a cylinder to an irregular shape. As the shear rate increased beyond the critical rate, at which the change in shape occurred, the degree of irregularity of the emerging stream increased [51].

As shown in Figure 11, the numerical simulation presents the volume fraction of the fluid in the system. As represented by the colour legend, the volume fraction in the LS equations varies from zero to one (blue to red). Note that when the value of the colour function is 1 (i.e. red), the system contains the polymer, and when the value of the volume fraction is 0 (i.e. blue), the system contains air. The interface of the two fluids is considered to be 0.5. The results of the TPF numerical simulations revealed that at higher inlet velocities and shear rates, certain instability of the polymer flow was observed. This result is consistent with the experimental observations. When the inlet velocity was below 145 mm·s<sup>-1</sup>, the polymer flow was stable and no deformation of the extrudate was observed. When the inlet velocity was increased, certain instabilities were observed. At the inlet velocity of 232 mm·s<sup>-1</sup>, the maximum shear rate in the system attained 2763 s<sup>-1</sup>. At this shear rate, instabilities were observed, appearing under wavy flow. Therefore, the numerical simulation reliably recreated the experimentally observed instabilities. By comparing the instability and wavy shape of the extrudate at

2763 s<sup>-1</sup> with the shape of the extrudate at higher shear rates, these instabilities were apparently thinner than those at higher shear rates. Thus, increasing the inlet velocity and shear rate highly influenced the stability and wavy shape of the extrudates owing to the variation in the shear rate and viscosity of the polymer along the liquefier radius. The difference between the viscosity at the centre and near the internal wall of the liquefier was high, thereby causing high extensional stress when the profile exits from the nozzle. This ‘sharkskin’ effect on the extrudate is typically observed for the extrusion of polymers [51] [52][53]. The ‘sharkskin’ is a defect that occurs as deep cracks on the surface of the extrudate. These cracks form during stress relaxation, causing a rough surface.

Inlet velocity (mm·s <sup>-1</sup> )	Shear rate (s <sup>-1</sup> )	Experimental study	Numerical simulation (volume fraction)	Magnified view	Colour legend
88	1561				
99	1753				
156	2763				

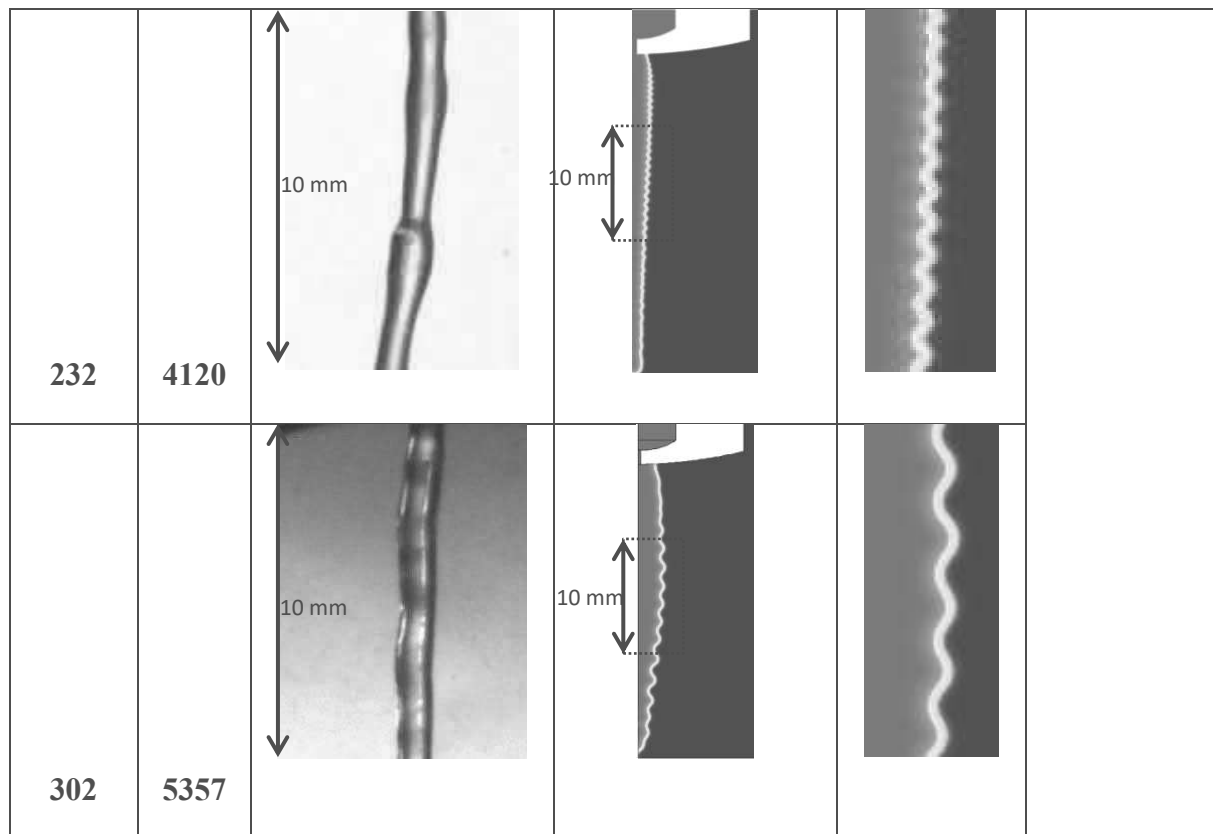


Figure 11: Influence of inlet velocity and shear rate on the shape of the extrudate exiting from the nozzle with a diameter of 0.5 mm

Based on the previous results, the following conditions are recommended for printing the PLA.

The printing temperature for the PLA must be higher than 190 °C to ensure a completely melted filament in the liquefier and prevent the clogging of the liquefier. However, the maximum temperature for printing must not exceed 210 °C. At temperatures higher than 210 °C, the viscosity of the polymer was excessively low, causing severe deformation during printing and degradation of the polymer. Moreover, the variation in the shear rate along the nozzle diameter should be reduced because it results in flow instabilities. We have observed that to achieve this condition, the temperature should be higher than 190 °C. Therefore, the recommended temperature is 200 °C.

To reduce the flow instabilities and surface defects, the shear rate during printing must be below 4000 s<sup>-1</sup>. The nozzle diameter highly influences the shear rate. That is, increasing the nozzle diameter decreases the shear rate. However, the nozzle diameter influences the roughness (surface quality) and precision of the manufactured parts. Increasing the nozzle diameter reduces the precision of the printed part. Therefore, to reduce the fluid instability and maintain the precision of the printed parts, a nozzle diameter of 0.4 mm or 0.5 mm is recommended.

The volume flow rate was determined on the basis of the feed rate and the geometry of the deposited bead, such as the height of the layer and width of the deposited bead. Therefore, the height of the deposited bead must not exceed 0.4 mm, and the feed rate must be below 30 mm·s<sup>-1</sup>.

## Conclusion

In this work, the FFF process applied to the PLA was investigated via experiments, analytical equations and numerical simulation. The effect of the printing parameters (i.e. nozzle diameter, feed

rate and layer height) and the physical properties of the polymer (i.e. thermal transitions and rheological behaviour) on the inlet velocity, shear rate and viscosity in the liquefier was determined.

Firstly, the maximum inlet velocity of the filament in the liquefier was empirically determined according to the printing parameters, such as the nozzle diameter, feed rate and dimensions of the deposited segment. Then, the rheological behaviour of the PLA, such as the velocity field, shear rate and viscosity distribution in the nozzle, was determined via analytical study and numerical simulation. The shear rate reached its maximum value near the internal wall at a high inlet velocity and small nozzle diameters. Increasing the inlet velocity and decreasing the nozzle diameter increased the shear rate and decreased the viscosity of the PLA. Meanwhile, reducing the viscosity enhanced the adhesion between the deposited beads and layers, and an excessively low viscosity resulted in low precision. Moreover, at the shear rates of higher than  $4000 \text{ s}^{-1}$ , the PLA extrudates underwent severe deformation caused by the 'sharkskin' effect. The deformation of the extrudate influenced the shape of the deposited beads and consequently reduced the control over the roughness and reliability of the manufactured part.

In parallel, a Multiphysics TPF model was developed to determine the viscosity of the polymer and shear rate according to various inlet velocities. Moreover, the numerical simulation was used to model the shape of the extrudate when it exits from the nozzle. The results obtained via numerical simulation were validated through experimental study. The numerical simulation focused on the shape of the deposited filament before deposition on the substrate for different flow regimes.

In the future work, the heat transfer and kinetics of crystallisation of the PLA must be numerically simulated. This work is a step towards optimising the printing conditions in the FFF process by using reliable parameters.

### **Acknowledgments**

This study received financial support from Université Fédérale de Toulouse and Occitanie region of France through a Ph.D. fellowship. The authors are grateful to François Grizet who first started studying 3D printing processes at ENIT-INP Toulouse. The authors would also like to thank Dr. Philippe Evon from Laboratoire de Chimie Agro-Industrielle – Université Fédérale de Toulouse for providing the PLA and guidance during its processing.

### **References:**

- [1] L. Novakova-Marcincinova, I. Kuric, Basic and Advanced Materials for Fused Deposition Modeling Rapid Prototyping Technology, *Manuf. Ind. Eng.* 11 (2012) 24–27.
- [2] C. Schelly, G. Anzalone, B. Wijnen, J.M. Pearce, Open-source 3-D printing technologies for education: Bringing additive manufacturing to the classroom, *J. Vis. Lang. Comput.* 28 (2015) 226–237. doi:10.1016/j.jvlc.2015.01.004.
- [3] "RepRap - RepRapWiki", Reprap.org, 2016. [Online]. Available: <http://reprap.org>. [Accessed: 14- Nov- 2016]., (2016).
- [4] M.A. Yardimci, Process analysis and planning for fused deposition modeling, University of Illinois at Chicago, Ph.D. Thesis, (1999).
- [5] M.A. Yardimci, D.I. Guceri, S.C. Danforth, Thermal analyse of Fused deposition modeling, in: 8th Solid Free. Fabr. Symp., University of Texas, (1996 ): pp. 689–698.

- [6] A.W. Fatimatuzahraa, B. Farahaina, W.A.. Yusoff, The effect of employing different raster orientations on the mechanical properties and microstructure of Fused Deposition Modeling parts, in: 2011 IEEE Symp. Business, Eng. Ind. Appl., Ieee, (2011): pp. 22–27. doi:10.1109/ISBEIA.2011.6088811.
- [7] J. De Ciurana, L. Serenó, È. Vallès, Selecting process parameters in RepRap additive manufacturing system for PLA scaffolds manufacture, *Procedia CIRP*. 5 (2013) 152–157. doi:10.1016/j.procir.2013.01.031.
- [8] B.M. Tymrak, M. Kreiger, J.M. Pearce, Mechanical properties of components fabricated with open-source 3-D printers under realistic environmental conditions, *Mater. Des.* 58 (2014) 242–246. doi:10.1016/j.matdes.2014.02.038.
- [9] J.C. Riddick, M.A. Haile, R. Von Wahlde, D.P. Cole, O. Bamiduro, T.E. Johnson, Fractographic analysis of tensile failure of acrylonitrile-butadiene-styrene fabricated by fused deposition modeling, *Addit. Manuf.* 11 (2016) 49–59. doi:10.1016/j.addma.2016.03.007.
- [10] A.K. Sood, R.K. Ohdar, S.S. Mahapatra, Experimental investigation and empirical modeling of FDM process for compressive strength improvement, *J. Adv. Res.* 3 (2012) 81–90. doi:10.1016/j.jare.2011.05.001.
- [11] B.H. Lee, J. Abdullah, Z. a. Khan, Optimization of rapid prototyping parameters for production of flexible ABS object, *J. Mater. Process. Technol.* 169 (2005) 54–61. doi:10.1016/j.jmatprotec.2005.02.259.
- [12] K. Thrimurthulu, P.M. Pandey, N. Venkata Reddy, Optimum part deposition orientation in fused deposition modeling, *Int. J. Mach. Tools Manuf.* 44 (2004) 585–594. doi:10.1016/j.ijmachtools.2003.12.004.
- [13] B. Wittbrodt, J.M. Pearce, The effects of PLA color on material properties of 3-D printed components, *Addit. Manuf.* 8 (2015) 110–116. doi:10.1016/j.addma.2015.09.006.
- [14] D. Ahn, J.-H. Kweon, S. Kwon, J. Song, S. Lee, Representation of surface roughness in fused deposition modeling, *J. Mater. Process. Technol.* 209 (2009) 5593–5600. doi:10.1016/j.jmatprotec.2009.05.016.
- [15] R. Anitha, S. Arunachalam, P. Radhakrishnan, Critical parameters in influencing the quality of prototypes in fused deposition modeling, *Journal of Materials Processing Technology*, 118 (2001) 385–388.
- [16] P. Vijay, P. Danaiah, K. V. D. Rajesh, Critical Parameters Effecting the Rapid Prototyping Surface Finish, *J. Mech. Eng. Autom.* 1 (2012) 17–20. doi:10.5923/j.jmea.20110101.03.
- [17] G. Percoco, F. Lavecchia, L.M. Galantucci, Compressive properties of FDM rapid prototypes treated with a low-cost chemical finishing, *Res. J. Appl. Sci. Eng. Technol.* 4 (2012) 3838–3842.
- [18] L.M. Galantucci, F. Lavecchia, G. Percoco, Quantitative analysis of a chemical treatment to reduce roughness of parts fabricated using fused deposition modeling, *CIRP Ann. - Manuf. Technol.* 59 (2010) 247–250. doi:10.1016/j.cirp.2010.03.074.
- [19] L.M. Galantucci, F. Lavecchia, G. Percoco, Experimental study aiming to enhance the surface finish of fused deposition modeled parts, *CIRP Ann. - Manuf. Technol.* 58 (2009) 189–192. doi:10.1016/j.cirp.2009.03.071.
- [20] S. Singamneni, A. Roychoudhury, O. Diegel, B. Huang, Modeling and evaluation of curved layer fused deposition, *J. Mater. Process. Technol.* 212 (2012) 27–35. doi:10.1016/j.jmatprotec.2011.08.001.

- [21] R.J.A. Allen, R.S. Trask, An experimental demonstration of effective Curved Layer Fused Filament Fabrication utilising a parallel deposition robot, *Addit. Manuf.* 8 (2015) 78–87. doi:10.1016/j.addma.2015.09.001.
- [22] P.M. Pandey, N.V. Reddy, S.G. Dhande, Improvement of surface finish by staircase machining in fused deposition modeling, *J. Mater. Process. Technol.* 132 (2003) 323–331.
- [23] D. Chakraborty, B. Aneesh Reddy, A. Roy Choudhury, Extruder path generation for Curved Layer Fused Deposition Modeling, *Comput. Aided Des.* 40 (2008) 235–243. doi:10.1016/j.cad.2007.10.014.
- [24] A.C. Abbott, G.P. Tandon, R.L. Bradford, H. Koerner, J.W. Baur, Process-structure-property effects on ABS bond strength in fused filament fabrication, *Addit. Manuf.* 19 (2018) 29–38. doi:10.1016/j.addma.2017.11.002.
- [25] G. Randall, *Sintering Theory and Practice*, Wiley-Interscience, New York, (1996).
- [26] C. Bellehumeur, L. Li, Q. Sun, P. Gu, Modeling of Bond Formation Between Polymer Filaments in the Fused Deposition Modeling Process, *J. Manuf. Process.* 6 (2004) 170–178. doi:10.1016/S1526-6125(04)70071-7.
- [27] S. Bakrani Balani, F. Chabert, V. Nassiet, A. Cantarel, C. Garnier, Toward improvement of the properties of parts manufactured by FFF ( Fused Filament Fabrication ) through understanding the influence of temperature and rheological behaviour on the coalescence phenomenon, in: *AIP Conf. Proc.* 1896, 040008, American Institute of Physics, (2017). doi:10.1063/1.5008034.
- [28] C. Pujos, Estimation de la rheologie d'un polymère dans une filière d'extrusion Simulation d'écoulement avec transferts thermiques et Inversion de mesures, L'universite Bordeaux 1, Ph.D. thesis, (2006). *In French*
- [29] V.W. Wang, C.A. Hieber, K.K. Wang, Dynamic simulation and graphics for the injection molding of three-dimensional thin parts, *J. Polym. Eng.* 7 (1986) 21–43.
- [30] F. Liravi, R. Darleux, E. Toyserkani, Additive manufacturing of 3D structures with non-Newtonian highly viscous fluids: Finite Element modeling and experimental validation, *Addit. Manuf.* 13 (2016) 113–123. doi:10.1016/j.addma.2016.10.008.
- [31] T. Köpplmayr, E. Mayrhofer, Numerical Simulation of Viscoelastic Layer Rearrangement in Polymer Melts using OpenFOAM, in: (2015). doi:10.1063/1.4918407.
- [32] R. Comminal, J. Spangenberg, J.H. Hattel, Numerical simulations of viscoelastic flows with free surfaces, *21em Congrès Français de Mécanique.* (2013) 1–6.
- [33] C. LE BOT, Impact et solidification de gouttes métalliques sur un substrat solide, L'universite de Bordeaux 1, Ph.D. Thesis, (2003). *In French*
- [34] A.D. Amico, A.M. Peterson, An adaptable FEA simulation of material extrusion additive manufacturing heat transfer in 3D, *Addit. Manuf.* 21 (2018) 422–430. doi:10.1016/j.addma.2018.02.021.
- [35] R. Jerez-Mesa, J.A. Travieso-Rodriguez, G. Gomez-Gras, X. Corbella, R. Busqué, Finite element analysis of the thermal behavior of a RepRap 3D printer liquefier, *Mechatronics.* 36 (2016) 119–126. doi:10.1016/j.mechatronics.2016.04.007.
- [36] R. Comminal, Numerical simulation of viscoelastic free surface flows using a streamfunction / log conformation formulation and the volume of fluid method, Technical University of Denmark, Ph.D. Thesis, (2015).

- [37] R. Comminal, M.P. Serdeczny, D.B. Pedersen, J. Spangenberg, Numerical modeling of the strand deposition flow in extrusion-based additive manufacturing, *Addit. Manuf.* 20 (2018) 68–76.
- [38] S. Bakrani Balani, A. Cantarel, F. Chabert, V. Nassiet, Influence of parameters controlling the extrusion step in Fused Filament Fabrication (FFF) process applied to polymers using numerical simulation, in: *AIP Conf. Proc.* 1960, 140003 (2018) doi:10.1063/1.5034995.
- [39] F. Peng, B.D. Vogt, M. Cakmak, Complex flow and temperature history during melt extrusion in material extrusion additive manufacturing, *Addit. Manuf.* 22 (2018) 197–206. doi:10.1016/j.addma.2018.05.015.
- [40] T.A. Osswald, J. Puentes, J. Kattinger, Fused filament fabrication melting model, *Addit. Manuf.* 22 (2018) 51–59. doi:10.1016/j.addma.2018.04.030.
- [41] C.S. Davis, K.E. Hillgartner, S. Hoon, J.E. Seppala, Mechanical strength of welding zones produced by polymer extrusion additive manufacturing, *Addit. Manuf.* 16 (2017) 162–166. doi:10.1016/j.addma.2017.06.006.
- [42] D.E. Henton, P. Gruber, J. Lunt, J. Randall, Polylactic Acid Technology, in: *Nat. Fibers, Biopolym. Biocomposites*, (2005): pp. 527–578. doi:10.1201/9780203508206.ch16.
- [43] D. Garlotta, A Literature Review of Poly Lactic Acid, *J. Polym. Environ.* 9 (2001) 63–84. doi:10.1023/A:1020200822435.
- [44] J.M. Dealy, J. Wang, *Melt Rheology and its Applications in the Plastics Industry*, Springer Science, 2 (2013). doi:10.1007/978-94-007-6395-1.
- [45] G. Schramm, *A Practical Approach to Rheology and Rheometry*, second edition, Gebrueder HAAKE GmbH, Karlsruhe, Karlsruhe, (1994).
- [46] J.F. Agassant, P. Avenas, B. Sergent, Jean, Philippe Vergnes, M. Vincent, *Mise en forme des polymères*, LAVOISIER, Paris, (2014).
- [47] J.F. Turner, A. Riga, A. O'Connor, J. Zhang, J. Collis, Characterization of drawn and undrawn poly-L-lactide films by differential scanning calorimetry, *J. Therm. Anal. Calorim.* 75 (2004) 257–268. doi:10.1023/B:JTAN.0000017347.08469.b1.
- [48] D. Battezzore, S. Bocchini, A. Frache, Crystallization kinetics of poly(lactic acid)-talc composites, *Express Polym. Lett.* 5 (2011) 849–858. doi:10.3144/expresspolymlett.2011.84.
- [49] R. Al-Itry, K. Lamnawar, A. Maazouz, Improvement of thermal stability, rheological and mechanical properties of PLA, PBAT and their blends by reactive extrusion with functionalized epoxy, *Polym. Degrad. Stab.* 97 (2012) 1898–1914.
- [50] M.F. Talbott, G.S. Springer, L.A. Berglund, The Effects of Crystallinity on the Mechanical Properties of PEEK Polymer and Graphite Fiber Reinforced PEEK, *J. Compos. Mater.* 21 (1987) 1056–1081. doi:10.1177/002199838702101104.
- [51] J.P. Tordella, An Instability in the Flow of Molten Polymers, *Rheol. Acta.* 3 (1958) 216–221.
- [52] J.M. Piau, J.F. Agassant, *Rheology for polymer melt processing*, Elsevier, (1996).
- [53] W.J. Schrenk, N.L. Bradley, T. Alfrey, Interfacial Flow Instability in Multilayer Coextrusion, *Polym. Eng. Sci.* 18 (1978) 620–623.